

1 **Supporting Information for**

2
3 **“Contrasting responses of different mixotrophic protists to light and nutrient**
4 **availability”**

5
6 Sebastiaan Koppelle^{1*}, Marina Ivanković^{2,3}, Mia M. Bengtsson⁴, Christian Preiler³, Jef
7 Huisman¹, Corina P.D. Brussaard^{1,5}, Julia C. Engelmann⁵, Robert Ptáčník³ & Susanne
8 Wilken^{1*}

9
10 ¹ Department of Freshwater and Marine Ecology (FAME), Institute for Biodiversity and
11 Ecosystem Dynamics (IBED), University of Amsterdam, P.O. Box 94920, 1090 GE
12 Amsterdam, the Netherlands

13 ² Department of Functional and Evolutionary Ecology, University of Vienna, Djerassiplatz 1,
14 1030 Vienna, Austria

15 ³ AquaScale lab, WasserCluster Lunz-Biologische Station GmbH, Dr. Carl Kupelwieser
16 Promenade, 5, A-3293, Lunz am See, Austria

17 ⁴ Institute of Microbiology, University of Greifswald, Felix-Hausdorff Strasse, 8, 17489,
18 Greifswald, Germany

19 ⁵ Department of Marine Microbiology and Biogeochemistry, NIOZ Royal Netherlands
20 Institute for Sea Research, P.O. Box 59, 1790 AB Den Burg, Texel, The Netherlands

21
22 * Corresponding authors: Sebastiaan Koppelle, s.koppelle@uva.nl ; Susanne Wilken,
23 s.wilken@uva.nl

24

25

26 **Materials and methods**

27 *Particulate and dissolved nutrient analysis*

28 Samples (15 mL) for soluble reactive phosphorus (SRP) and dissolved inorganic nitrogen
29 (DIN; $\text{NO}_x + \text{NH}_4^+$) were filtered over pre-combusted (450 °C, 4 h) and acid washed (in 10-
30 15% HCl followed by 5 washes MilliQ water) glass fiber filters (25 mm diameter, GF/F,
31 Whatman[®], Cytiva, Marlborough, Massachusetts, USA) and measured directly after
32 collection. SRP was measured by the ascorbic acid method (Hansen and Koroleff 1999) on a
33 UV-1900 spectrophotometer (Shimadzu, Kyoto, Japan; detection limit: 0.04 $\mu\text{g L}^{-1}$).
34 Ammonium, nitrate and nitrite concentrations were measured on a FLOWSYS continuous
35 flow analyzer (Alliance Instruments, Salzburg, Austria, detection limits: $\text{N-NH}_4^+ = 2 \mu\text{g L}^{-1}$,
36 $\text{N-NO}_3^- = 100 \mu\text{g L}^{-1}$, $\text{N-NO}_2^- = 1 \mu\text{g L}^{-1}$). Ammonium concentrations were determined by the
37 indophenol blue method, nitrate by the hydrazine reduction method and nitrite by the
38 colorimetric method (Rice et al. 2012). To determine the nutrient stoichiometry of the
39 experimental community, water samples (~500 mL) were filtered onto pre-combusted and
40 acid-washed glass fiber filters (25 mm diameter, GF/F, Whatman[®], Cytiva, Marlborough,
41 Massachusetts, USA) for analysis of particulate organic carbon (POC) and nitrogen (PON), as
42 well as total particulate phosphorus (TPP). Filters were stored at -80 °C until further
43 processing. For analysis of POC and PON filters were freeze dried for 24 h, amended with
44 several drops of 4 mol L^{-1} HCl (Sigma-Aldrich, St. Louis, Missouri, USA) to remove
45 remaining inorganic carbon, and left to dry overnight on a heating plate (40°C). Filters were
46 then folded into silver foil (Elementar Analysensysteme GmbH, Langenselbold, Germany)
47 and POC and PON were measured using a CHNS elemental analyser (1050 °C, VarioEL
48 Cube, Elementar Analysensysteme GmbH, Germany) with sulfanilic acid as standard (5-10
49 mg, S387444, Sigma-Aldrich, St. Louis, Missouri, USA). Samples for the analysis of TPP
50 were combusted (450 °C, 4 h), extracted with dilute sulphuric acid (Solórzano and Sharp,

51 1980) and quantified as described for SRP.

52

53 *Chlorophyll a and analysis of phytoplankton community composition by microscopy*

54 For determination of chl-*a* concentrations samples were filtered onto glass fiber filters (25
55 mm diameter, GF/F, Whatman[®], Cytiva, Marlborough, Massachusetts, USA), and stored
56 frozen until their extraction in acetone and spectrophotometric analysis according to Parsons
57 et al. (1984). The composition of the eukaryotic phytoplankton community present in the
58 experimental incubations was analyzed microscopically in samples (45 mL) fixed with acidic
59 Lugol's iodine solution (1% v/v final concentration). Sample storage and determination of
60 cellular abundances and biovolumes were as described in Koppelle et al. (2022).

61

62 *Eukaryotic phytoplankton community composition*

63 For analysis of community composition based on 18S rRNA gene amplicon sequences,
64 samples from both the experiment and time-series were filtered onto 0.2 µm pore size Supor[®]
65 polyether sulfone (PES) membrane filters (Pall Corporation, Washington, USA) and stored at
66 -80 °C until further processing. DNA samples from the experiment were extracted using the
67 Qiagen DNeasy Plant kit according to the manufacturers protocol with the addition of a
68 mechanical lysis step. For this, DNA filters were transferred to a 2 mL screw cap tube
69 containing 400 µL lysis buffer and ~100 µL of glass beads (0.1 mm + 0.5 mm in a 1:1 ratio)
70 and homogenized in a beat-beater (Precellys[®] 24, Bertin instruments, France) for 2 min at a
71 stroke frequency of 100 s⁻¹. Additionally, the samples were subjected to three rounds of
72 freezing and thawing by flash freezing in liquid nitrogen before thawing on a heating plate at
73 65 °C. Samples from the time-series were extracted using the Qiagen DNeasy Powersoil Pro
74 kit according to the manufacturers protocol with bead-beating pre-cut filters in a Retsch MM2
75 swing mill (Retsch GmbH, Haan, Germany) for 5 min at a stroke frequency of 70 s⁻¹ as

76 additional mechanical lysis step. Following extractions, DNA concentrations were quantified
77 using a Qubit™ 2.0 fluorometer according to manufacturer instructions (Invitrogen,
78 ThermoFisher™ Scientific, USA).

79 The V7 hypervariable region of the 18S rRNA gene was amplified for both
80 experimental and time-series samples using the F-1183mod/R-1443mod primer pair
81 (Hadziavdic et al. 2014). Additionally, the V4 hypervariable region was amplified for
82 experimental samples using the TAREuk454FWD1/V4RB primer pair (Balzano et al. 2015).
83 All primers were ligated to an Illumina adapter sequence at their 5' end. PCR reactions
84 included 1x Phusion™ buffer, 200 µmol L⁻¹ dNTP's, 0.35 µmol L⁻¹ of each primer, 1U
85 Phusion™ high-fidelity DNA polymerase (F530S, ThermoFisher™ Scientific, USA) and 2.5
86 ng of template DNA in a total volume of 50 µL. The PCR program consisted of an initial
87 denaturation step at 98 °C for 2 min followed by 25 cycles of 10 sec at 98 °C, 30 sec at 50 °C
88 (for V4) or 60 °C (for V7), 30 sec at 72 °C, and a final extension at 72 °C for 10 min. PCR
89 products were cleaned using the Qiagen MinElute® PCR purification kit (Qiagen, Germany).
90 Experimental samples were sequenced at Eurofins Genomics Germany GmbH (Ebersberg,
91 Germany) using the Illumina NovaSeq for the V7 amplicons (2 x 150bp) and Illumina MiSeq
92 with v3 chemistry (2x300 bp) for the V4 amplicons. For time-series samples, V7 amplicons
93 were sequenced on an Illumina MiSeq (v3, 2x300 bp), and library preparation and sequencing
94 were carried out by LGC Genomics (Berlin, Germany). After demultiplexing, and barcode
95 and primer removal, V4 and V7 sequences were individually processed using DADA2 in
96 Qiime2 (version 2022.2, default settings, Callahan et al. 2016). As overall read quality was
97 high a threshold phred score of 30 was used before trimming with truncation lengths of 123
98 nts and 135 nts for the forward and reverse reads, respectively, resulting in an average overlap
99 of at least 30 nucleotides. After merging and denoising, taxonomic classification of amplicon
100 sequence variants (ASVs) was performed using the Qiime2 feature-classifier plugin with

default parameter settings (k-mer range 7.7, confidence 0.7) and trained on only the V4 or V7 regions of the 18S rRNA genes from the PR2 database (version 4.14, Guillou et al. 2013) using a naïve Bayes classification approach (Bokulich et al. 2018).

Epifluorescence microscopy

For enumeration of bacterial abundances, 2 mL subsamples were filtered onto white polycarbonate filters of 25 mm diameter and 0.2 µm pore-size (Whatman®, Cytiva, Marlborough, Massachusetts, USA). The filters were air dried, and mounted on a microscope slide using Vectashield® mounting medium (Vector Laboratories, Newark, New Jersey, USA) containing 4',6-diamidino-2-phenylindole (DAPI). For determination of protistan grazing rates, 30 mL sample was filtered onto 3 µm pore-size polycarbonate filters (25 mm diameter, Whatman®), and mounted as described above. Filters were stored at -20 °C until analysis by epifluorescence microscopy. Bacteria were enumerated on a Zeiss Axioskop II at 1000x magnification using Zeiss filter set 02 (excitation filter G365, beam splitter FT395, emission filter LP420) for DAPI stained bacteria and filter set 10 (excitation filter BP450-490, beam splitter FT510, emission filter BP515-565) for FLBs. Protist cells were visualized at 1000x magnification using DAPI excitation (filter set 02). To distinguish heterotrophic protists from mixotrophic protists, cells were checked for the presence of chlorophyll autofluorescence and ingested FLB using Zeiss filter set 09 (excitation filter BP450-490, beam splitter FT510, emission filter LP515). Due to their overall low abundance ~90 *Pseudopedinella*-like dictyochophytes and ~200 'large' cryptophytes (> 20 µm) were counted per filter in an average of 2400 randomly distributed fields of view. The 'small' cryptophytes (5 – 20 µm) were more abundant and 300 – 400 cells were counted per filter in an average of ~650 randomly distributed fields of view.

Estimation of nutritional gains by bacterivory

To estimate the contribution of bacterivory by cryptophytes and *Pseudopedinella*-like dictyochophytes to their respective carbon, nitrogen and phosphorus needs, first the average biovolume of ingested natural bacteria was calculated using microscopic size measurements and standard equations for rod and coccoid shaped bacteria. Bacterial biovolume was then converted to C, N and P content using the biovolume-to-carbon equation by Norland (1993) and C:N and C:P conversions from Fagerbakke et al. (1996), and multiplied by grazing rates to obtain an estimated total C, N, and P gain per protist. Subsequently, the average protistan biovolume was calculated using conversion formulae as provided on www.planktonforum.eu (*Pseudopedinella*: spherical; small cryptophyte: cone with half a sphere; large cryptophyte: flattened ellipse) and converted to carbon content using the protistan carbon-to-volume equation of Menden-Deuer and Lessard (2000). Nitrogen and phosphorus content were then estimated assuming Redfield ratio (C:N:P = 106:16:1; Moorthi et al. 2017). Finally, the daily C/N/P gain from bacterivory was expressed as percentage of the protistan C/N/P content.

Depth-volume integrated sampling (DVI)

To obtain a single sample representative for the phytoplankton community in Lake Lunz, a depth-volume-integrated (DVI) sample was collected, based on the lake's hypsographic curve. The DVI sample is composed of water samples collected at 10 fixed discrete depths (see Figure S1 below). Each of these 10 water samples corresponds to a given depth range (e.g. 1 m represent 0-2 m; 3 m represents 2-4 m and so on). A representative sample was then obtained by mixing water from the 10 different depths proportional to the lake volume represented by each depth interval. Abundance of a given taxon in the DVI sample is thus proportional to the total population size in the lake, irrespective of its vertical distribution. This exact method has been used starting in March 2017. Prior, the share of an individual

sample in the DVI sample reflected the lake area in the respective depth (shown on the x-axis in Figure S1).

Phylogenetic analysis

Reference sequences representing all major clades within the cryptophytes and dictyochophytes (118 and 73 sequences, respectively) were obtained from the literature and the NCBI NT database (Hoef-Emden 2008; Greenwold et al. 2019; Choi et al. 2020; Hamilton et al. 2021; <https://www.ncbi.nlm.nih.gov/nucleotide/>). Sequences were aligned in MEGA X (Kumar et al. 2018) using MUSCLE and trimmed to a total length of 1457 and 1592 nucleotides for cryptophytes and dictyochophytes, respectively. Subsequently, a maximum likelihood phylogenetic tree was computed for each group on the IQTree 2 web server (Nguyen et al. 2015; Minh et al. 2020). Using the -m MFP command (Kalyaanamoorthy et al. 2017) the best fitting substitution models were calculated to be the Tamura-Nei 93 (TN; cryptophytes) and the General Time Reversible model (GTR; dictyochophytes) with a discrete gamma distribution and evolutionary invariant sites (+G+I). Gaps were treated as complete deletion and branch support was calculated based on single branch tests (SH-aLRT, -alrt 1000) in combination with ultrafast bootstrap approximation (-bb 1000; Hoang et al. 2018), both with 1000 replicates. Finally, both ML trees were rooted on their outgroup (five katablepharid species for cryptophytes (*Leucocryptos marina* clone 3902, *Hatena arenicola* HY-051, *Katablepharis japonica* AB231617, *K. remigera* AY919672, uncultured Katablepharid KF761288) and three pelagophytes for dictyochophytes (*Aureococcus anophagefferens* BH56 189 (KY980308), *Pelagomonas calceolata* NIES-3883 (LC189147), uncultured Pelagophyte WS071.069 (KP404700)).

177 *Statistical analysis of time-series data*

178 Schmidt's stability index was calculated from temperature profiles and the lake's
179 hypsographic curve using the R package rLakeAnalyzer (version 1.11.4.1). Prior to
180 regression analyses, Pearson's correlation coefficients were calculated to assess potential
181 collinearity between environmental parameters. Individual linear regression models were then
182 built for each dictyochophyte and cryptophyte ASV of interest (clr-transformed counts) with
183 the remaining environmental parameters (chl-*a*, SRP, NO₃⁻, NH₄⁺, Secchi depth, Schmidt's
184 stability index) as explanatory variables. The best regression model was determined starting
185 from the full regression model and using stepAIC of the MASS package (version 7.3.58.1,
186 Venables and Ripley, 2002) for stepwise deletion of the least significant explanatory variable.
187 The model with the lowest Akaike information criterion (AIC) score was selected as the best
188 model.

189 **Table S1.** Feature IDs obtained from the analysis of 18S rRNA gene amplicons from the grazing experiment, and their matching ASV and
190 species names as used in this study. The feature IDs obtained from the grazing experiment (V4/V7) as well as the time-series can be traced back
191 to the ASV tables as archived in the online repository (Figshare: doi:10.21942/uva.23859318). The feature IDs from the time series are those
192 ASVs that had a 100% match with the ASVs obtained from the V7 hypervariable region in the grazing experiment.

<i>Cryptophytes</i>					
Feat. ID Experiment (V4)	Feat. ID Experiment (V7)	Feat. ID Time-series	ASV name (V4)	ASV name (V7)	Species name
95fc6f51a14b2ceb28f627ef34e3e3d6	52fae5f8f5bf8120c37769da3c9459c2	ASV62	C4.4	C7.1	<i>C. marssonii</i>
df8d39f8d829def283f5fee8eba9818b	7747096724c4953c3d062360de232fbd	ASV27	C4.6	C7.2	<i>C. tetrapyrenoidosa</i>
a751a380a0f1851052cd89844ca9ff9a	8ae649c35aaa9c9b52075ba6ff477503	ASV110	C4.5	C7.3	<i>C. pyrenoidifera</i>
61e5e97a79704872015885e4d97db8f7	b2b46ffa92e44def7b2636d632c9f5a1	ASV69	C4.8	C7.4	<i>R. minuta</i>
289122710ece2a6762836db77d99f779	b9a3632fa179fbcaf4cfb56eb806adbd	ASV19	C4.1	C7.5	<i>P. nannoplanctica</i>
098ee65c036cd9ff2c48e25e5f7c08c1			C4.7		
58c2f256268a80263e699cf1463c3ac2	ed03b29985ea280db68b04c574777231	ASV2	C4.2	C7.6	<i>C. curvata</i>
6da3784cb3719666d42f9b1862a51116			C4.3		
<i>Dictyochophytes</i>					
Feat. ID Experiment (V4)	Feat. ID Experiment (V7)	Feat. ID Time-series	ASV name (V4)	ASV name (V7)	Species name
e860d1d205018497f674233e5755cbeb	75850d7c8d955ffc3149cbf9804a1a56	ASV120	D4.3	D7.1	<i>Pseudopedinella sp.</i>
b1ac79d1759d884c75f46d21961f9f6a	9b83e9888ac259103df2fdae0bcb8a1f	ASV183	D4.4	D7.2	<i>Uncultured Pedinellales – 2</i>
01b1e603e6110b85274f1b3c8c5256c8	9dde918ea73a462cedb0af59d7825dcb	ASV130	D4.1	D7.3	<i>Uncultured Pedinellales - 1</i>
82a1561c2e9ba430f22b4a8f8e84ae63			D4.2		

194 **Table S2.** Nutrient conditions in Lake Lunz during collection of the experimental community
 195 (from 3 m depth) on August 20, 2020. Data show mean \pm 1 standard deviation ($n = 3$).

Nutrient	Concentration ($\mu\text{g L}^{-1}$)
SRP	0.50 ± 0.04
N-NO ₃	464.90 ± 2.72
N-NH ₄	< DL*
N-NO ₂	6.57 ± 0.35
POC	365.15 ± 11.79
PON	106.13 ± 6.12
POP	6.56 ± 0.26
Nutrient ratios	Molar ratio
DIN:DIP	2104 ± 159
POC:PON	4.03 ± 0.35
POC:POP	143.81 ± 7.72

196

197 * Below the detection limit (DL) of $2 \mu\text{g L}^{-1}$

198 **Table S3.** Results of the two-way ANOVAs performed to test the effect of light and
199 phosphorus on percentage of feeding cells (%) and (estimated) cell-specific grazing rates
200 ((e)CSGR) for *Pseudopedinella*-like flagellates, small cryptophytes and large cryptophytes.
201 Significant p-values are indicated in bold.

	Df	Sum of Squares	Mean sum of Squares	F	p-value
<i>Percentage feeding (%)</i>					
Small cryptophytes					
Factor					
Light	1	33.81	33.81	14.84	< 0.01
Phosphorus	1	13.52	13.52	5.94	0.03
Light * Phosphorus	1	8.74	8.74	3.84	0.07
Residuals	15	34.17	2.28		
Large cryptophytes					
Factor					
Light	1	85.96	85.96	12.63	< 0.01
Phosphorus	1	65.50	65.60	9.64	< 0.01
Light * Phosphorus	1	13.72	13.72	2.02	0.18
Residuals	15	102.07	6.80		
<i>Pseudopedinella</i>-like flagellates					
Factor					
Light	1	35.0	34.99	1.09	0.31
Phosphorus	1	20.0	19.97	0.62	0.44
Light * Phosphorus	1	20.1	20.07	0.63	0.44
Residuals	15	481.0	-32.06		
<i>(e)CSGR</i>					
Small cryptophytes					
Factor					
Light	1	0.11	0.11	4.86	0.04
Phosphorus	1	0.02	0.02	0.97	0.34
Light * Phosphorus	1	0.07	0.07	2.97	0.11
Residuals	15	0.35	0.02		
Large cryptophytes					
Factor					
Light	1	22.02	22.02	23.67	< 0.001
Phosphorus	1	14.09	14.09	15.15	< 0.01
Light * Phosphorus	1	3.04	3.04	3.27	0.09
Residuals	15	13.95	0.93		
<i>Pseudopedinella</i>-like flagellates					
Factor					
Light	1	1.23	1.23	0.21	0.67
Phosphorus	1	0.50	0.50	0.08	0.78
Light * Phosphorus	1	9.81	9.81	1.64	0.22
Residuals	15	89.5	5.97		

203 **Table S4.** Post-hoc comparison of the means using Tukey HSD, after the two-way ANOVAs
 204 (Table S3). Significant p-values are indicated in bold. Treatments: in-situ conditions (control),
 205 phosphorus addition (+P), low light intensity (LL) and low light with phosphorus addition
 206 (LL+P).

	Difference	p-value	Difference	p-value
	<i>Percentage feeding (%)</i>		<i>(e)CSGR</i>	
Small cryptophytes				
Pairwise comparison				
Control vs. +P	-3.14	0.03	-0.20	0.26
Control vs. LL	3.86	< 0.01	0.26	0.06
Control vs. LL + P	-4.27	< 0.01	-0.22	0.15
+P vs. LL	0.73	0.89	0.07	0.91
+P vs. LL + P	1.14	0.68	0.02	0.99
LL vs. LL + P	-0.41	0.97	0.04	0.97
Large cryptophytes				
Pairwise comparison				
Control vs. +P	-5.54	0.03	-2.58	< 0.01
Control vs. LL	5.66	0.02	2.82	< 0.01
Control vs. LL + P	-7.78	< 0.01	-3.79	< 0.0001
+P vs. LL	0.13	0.99	0.24	0.98
+P vs. LL + P	2.25	0.59	1.21	0.28
LL vs. LL + P	-2.12	0.59	-0.97	0.41
<i>Pseudopedinella</i>-like flagellates				
Pairwise comparison				
Control vs. +P	0.13	0.99	1.20	0.88
Control vs. LL	0.66	0.99	0.87	0.94
Control vs. LL + P	-4.66	0.58	-0.82	0.95
+P vs. LL	0.79	0.99	0.34	0.99
+P vs. LL + P	4.79	0.60	2.02	0.62
LL vs. LL + P	-4.00	0.69	-1.69	0.70

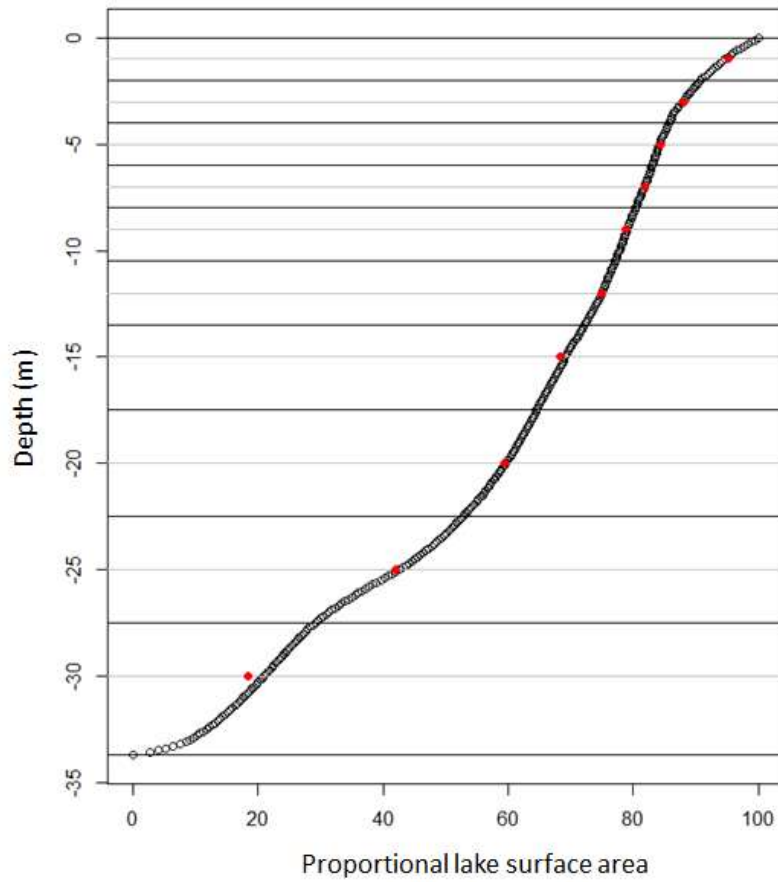
207

208 **Table S5.** Estimated C, N, and P content of mixotrophic predators and nutritional gains from
 209 feeding on bacterial prey by *Pseudopedinella*-like flagellates, and cryptophytes. Treatments:
 210 in-situ conditions (control), phosphorus addition (+P), low light intensity (LL) and low light
 211 with phosphorus addition (LL+P). Average CNP content of natural bacterial prey was
 212 estimated from their cell size ($\sim 0.9 \mu\text{m}$) resulting in $0.036 \text{ pg C cell}^{-1}$, $0.007 \text{ pg N cell}^{-1}$, and
 213 $0.001 \text{ pg P cell}^{-1}$. As FLB cell dimensions were not scored from the grazing experiment, the
 214 average CNP content of natural bacterial prey was used for nutritional gain calculations. Data
 215 show mean ± 1 standard deviation.
 216

	C/N/P content protist (pg cell^{-1})			C/N/P gain from bacteria ($\text{pg cell}^{-1} \text{ d}^{-1}$)		
	C	N	P	C	N	P
Small cryptophytes						
Control	23.6 ± 4.5	3.6 ± 0.7	0.22 ± 0.04	0.5 ± 0.2	0.11 ± 0.04	0.02 ± 0.01
+P	19.5 ± 4.7	2.9 ± 0.7	0.18 ± 0.04	0.4 ± 0.1	0.07 ± 0.02	0.01 ± 0.00
LL	22.6 ± 3.1	3.4 ± 0.5	0.21 ± 0.03	0.3 ± 0.1	0.06 ± 0.01	0.01 ± 0.00
LL + P	26.0 ± 9.9	3.9 ± 1.5	0.25 ± 0.09	0.4 ± 0.1	0.07 ± 0.02	0.01 ± 0.00
Large cryptophytes						
Control	394.6 ± 72.2	59.6 ± 10.9	3.72 ± 0.68	7.9 ± 1.0	1.59 ± 0.21	0.30 ± 0.04
+P	396.7 ± 64.8	59.9 ± 9.8	3.74 ± 0.61	5.6 ± 0.9	1.13 ± 0.17	0.22 ± 0.03
LL	364.8 ± 69.2	55.1 ± 10.4	3.44 ± 0.65	5.4 ± 0.7	1.08 ± 0.14	0.21 ± 0.03
LL + P	239.4 ± 11.2	36.1 ± 1.7	2.26 ± 0.11	4.5 ± 0.8	0.91 ± 0.16	0.17 ± 0.03
<i>Pseudopedinella</i>-like flagellates						
Control	43.5 ± 4.6	6.6 ± 0.7	0.41 ± 0.04	7.1 ± 1.5	1.43 ± 0.31	0.27 ± 0.06
+P	49.2 ± 3.3	7.4 ± 0.5	0.46 ± 0.03	8.1 ± 2.4	1.62 ± 0.48	0.31 ± 0.09
LL	53.0 ± 6.5	8.0 ± 1.0	0.50 ± 0.06	7.8 ± 2.3	1.57 ± 0.46	0.30 ± 0.09
LL + P	32.2 ± 4.2	4.9 ± 0.6	0.30 ± 0.04	6.5 ± 1.5	1.30 ± 0.31	0.25 ± 0.06

Table S6. Output of the significance test using the RAIN package in R on amplicon abundance and environmental parameter seasonal dynamics. RAIN output gives the phase, peak shape, period tested for and the significance of the rhythm (p-value). The phase is the time in the tested period with peak abundance. Peak shape illustrates the shape and symmetry of the peak expressed as the part of the tested period that has a ‘falling’ slope (e.g. peak shape of 9 implies that, in total, 9 out of 12 months showed a falling slope and hence 3 out of 12 months showed a rising slope). The tested period was 12 months (e.g. 1 = January, 12= December) to test for an annual periodicity in the clr-transformed amplicon abundances of the most dominant cryptophyte and dictyochophyte ASVs. Significant p-values are indicated in bold ($p < 0.05$).

ASV	Species name	Phase (month of peak abundance)	Peak shape	Period (months)	p-value
ASV C7.1	<i>C. marssonii</i>	1	3	12	< 0.001
ASV C7.2	<i>C. tetrapyrenoidosa</i>	10	6	12	0.041
ASV C7.3	<i>C. pyrenoidifera</i>	10	6	12	< 0.001
ASV C7.4	<i>R. minuta</i>	3	5	12	0.008
ASV C7.5	<i>P. nannoplantica</i>	12	8	12	< 0.001
ASV C7.6	<i>C. curvata</i>	10	8	12	0.039
ASV D7.1	<i>Pseudopedinella sp.</i>	5	9	12	< 0.001
ASV D7.2	Uncultured Pedinellales - 2	4	7	12	0.018
ASV D7.3	Uncultured Pedinellales - 1	5	9	12	< 0.001
Environmental parameter					
Chlorophyll- <i>a</i>		5	6	12	0.002
Schmidt stability		8	7	12	<0.001
Secchi depth		12	4	12	<0.001
NH ₄ ⁺		8	7	12	<0.001
SRP		1	5	12	0.009
NO ₃ ⁻		4	4	12	<0.001



228

229 **Figure S1.** Hypsographic curve of Lake Lunz. Black dots represent the volumetric depth
 230 profile of the lake (10 cm interval), red dots are the discrete samples representing the 10
 231 different depth ranges of the lake (indicated by the black horizontal lines).

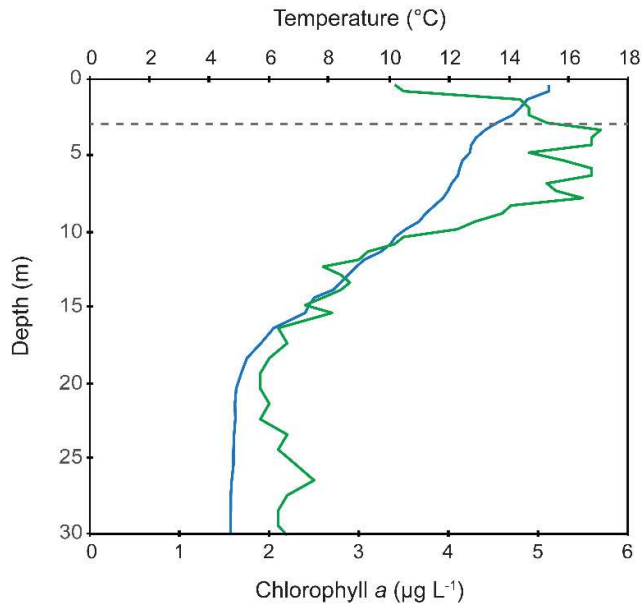


Figure S2. Temperature (blue) and chlorophyll *a* (green) profiles of Lake Lunz on the day of the grazing experiment. The dashed line indicates the sampling depth (3 m) at which lake water was collected for the grazing experiment.

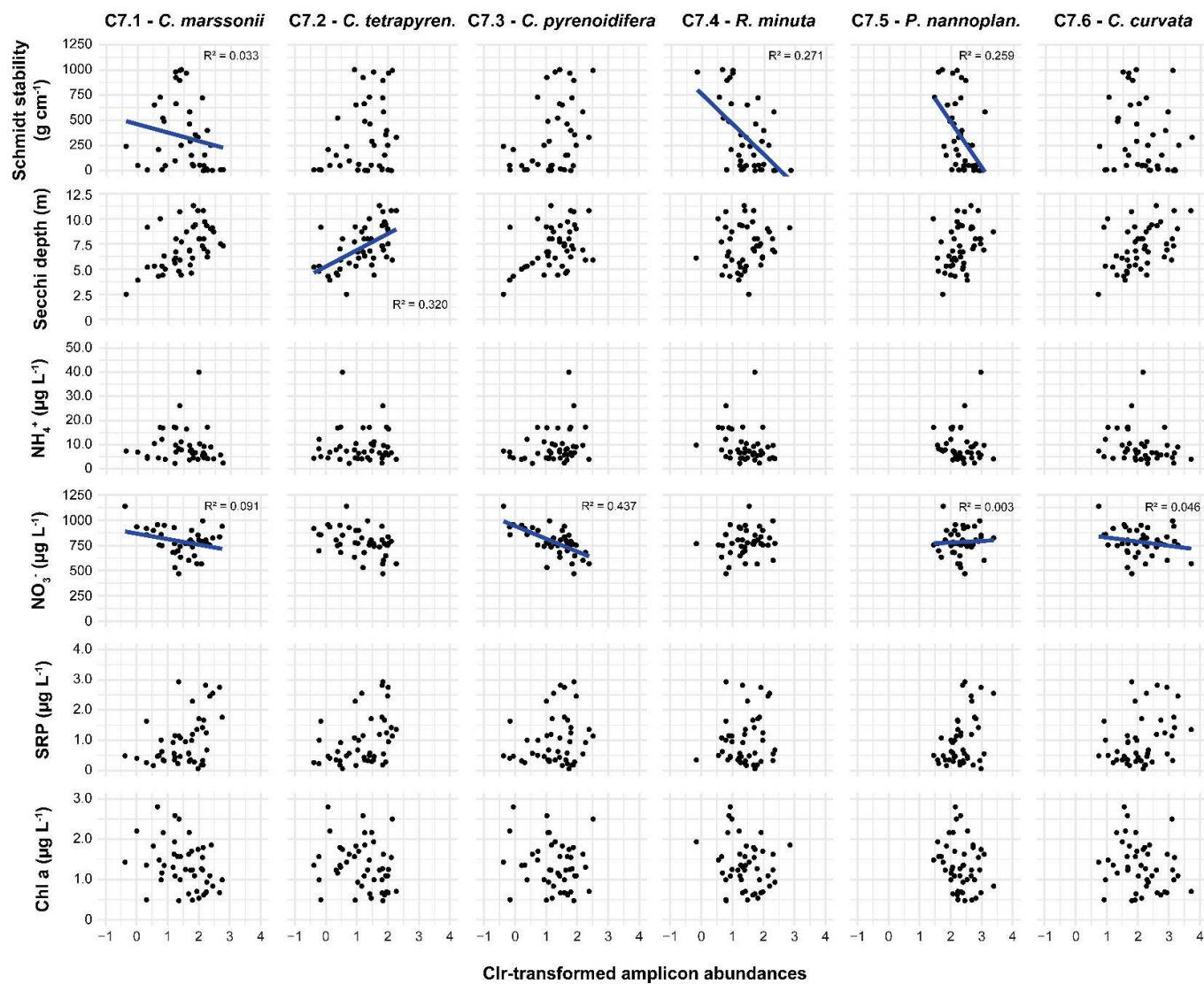
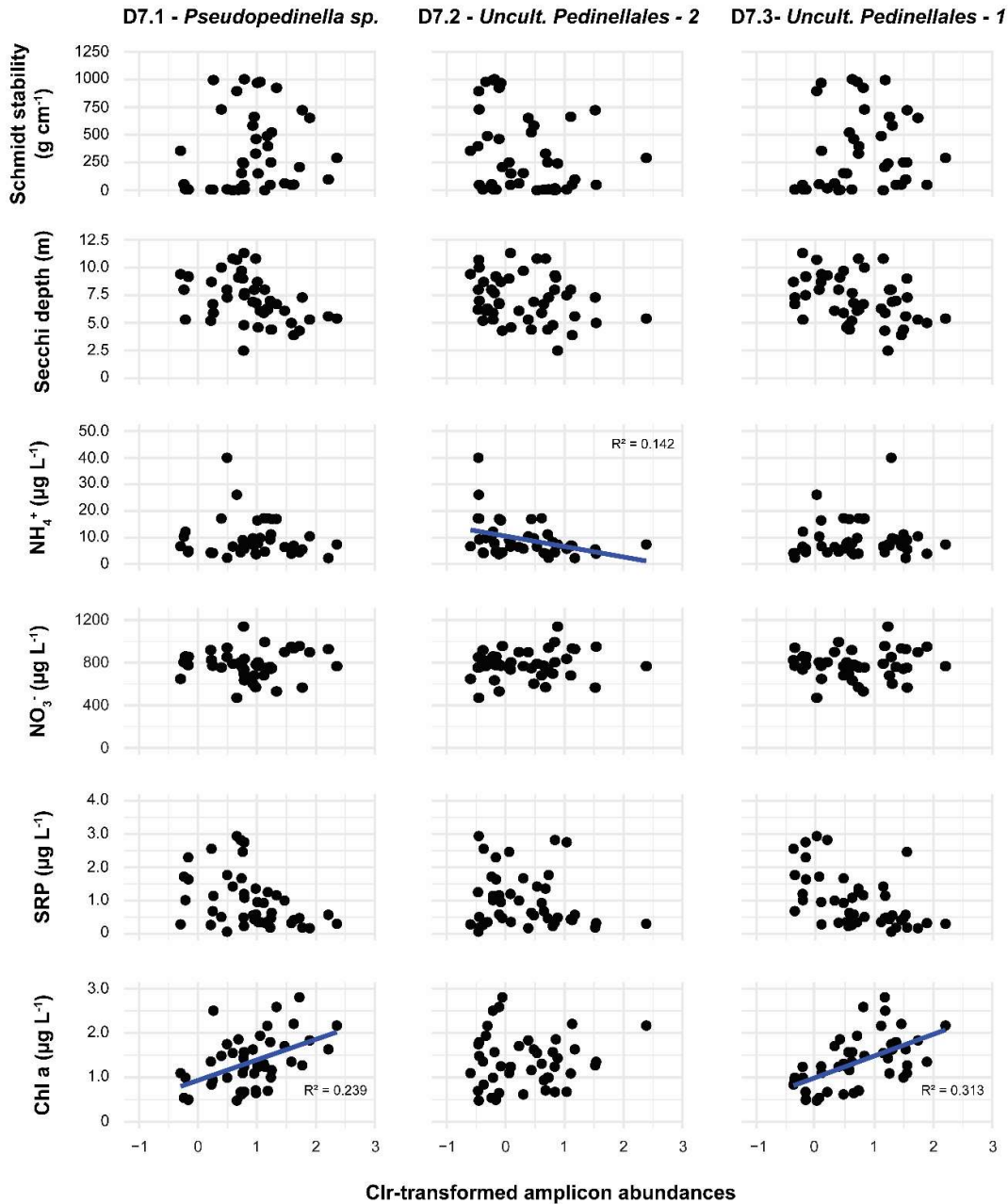


Figure S3. Biplots of the relationships between cryptophyte ASV dynamics (clr-transformed amplicon abundances) and environmental parameters. For those parameters, which the multiple linear regression analysis identified as significant (Table 3 in manuscript), a linear regression line and R^2 value was included. As the biplots here reflect simply the direct relation between the ASV dynamics and an individual environmental parameter, they differ from the multiple linear regression analyses in the manuscript.



245

246 **Figure S4.** Biplots of the relationships between dictyochophyte ASV dynamics (clr-
 247 transformed amplicon abundances) and environmental parameters. For those parameters,
 248 which the multiple linear regression analysis identified as significant (Table 3 manuscript), a
 249 linear regression line and R² value was included. As the biplots here reflect simply the direct
 250 relation between the ASV dynamics and an individual environmental parameter, they differ
 251 from the multiple linear regression in the manuscript.

252 **References**

- 253 Balzano, S., E. Abs, and S. C. Leterme. 2015. Protist diversity along a salinity gradient in a
254 coastal lagoon. *Aquat. Microb. Ecol.* **74**: 263–277. doi:10.3354/ame01740
- 255 Bokulich, N. A., B. D. Kaehler, J. R. Rideout, M. Dillon, E. Bolyen, R. Knight, G. A. Huttley,
256 and J. Gregory Caporaso. 2018. Optimizing taxonomic classification of marker-gene
257 amplicon sequences with QIIME 2’s q2-feature-classifier plugin. *Microbiome* **6**: 90.
258 doi:10.1186/s40168-018-0470-z
- 259 Callahan, B. J., P. J. McMurdie, M. J. Rosen, A. W. Han, A. J. A. Johnson, and S. P. Holmes.
260 2016. DADA2: High-resolution sample inference from Illumina amplicon data. *Nat.*
261 *Methods* **13**: 581–583. doi:10.1038/nmeth.3869
- 262 Choi, C. J. and others. 2020. Seasonal and geographical transitions in eukaryotic
263 phytoplankton community structure in the Atlantic and Pacific oceans. *Front. Microbiol.*
264 **11**: 542372. doi:10.3389/fmicb.2020.542372
- 265 Fagerbakke, K. K. M., M. Heldal, and S. Norland. 1996. Content of carbon, nitrogen, oxygen,
266 sulfur and phosphorus in native aquatic and cultured bacteria. *Aquat. Microb. Ecol.* **10**:
267 15–27. doi:https://doi.org/10.3354/ame010015
- 268 Greenwold, M. J., B. R. Cunningham, E. M. Lachenmyer, J. M. Pullman, T. L. Richardson,
269 and J. L. Dudycha. 2019. Diversification of light capture ability was accompanied by the
270 evolution of phycobiliproteins in cryptophyte algae. *Proc. R. Soc. B Biol. Sci.* **286**:
271 20190655. doi:10.1098/rspb.2019.0655
- 272 Guillou, L. and others. 2013. The Protist Ribosomal Reference database (PR2): A catalog of
273 unicellular eukaryote Small Sub-Unit rRNA sequences with curated taxonomy. *Nucleic*
274 *Acids Res.* **41**: 597–604. doi:10.1093/nar/gks1160

275 Hadziavdic, K., K. Lekang, A. Lanzen, I. Jonassen, E. M. Thompson, and C. Troedsson. 2014.
 276 Characterization of the 18S rRNA gene for designing universal eukaryote specific
 277 primers. PLoS One **9**: e87624. doi:10.1371/journal.pone.0087624

278 Hamilton, M., M. Mascioni, E. Hehenberger, C. Bachy, C. Yung, M. Vernet, and A. Z.
 279 Worden. 2021. Spatiotemporal variations in antarctic protistan communities highlight
 280 phytoplankton diversity and seasonal dominance by a novel cryptophyte lineage. MBio
 281 **12**: e02973-21. doi:10.1128/mBio.02973-21

282 Hansen, H. P., and, F. Koroleff. 1999. Determination of nutrients. In: K. Grasshoff, K.
 283 Kremling, and M. Ehrhardt (Eds.), Methods of Seawater Analysis 3rd ed. Weinheim,
 284 German, Wiley-VCH Verlag GmbH, 159–228.

285 Hoang, D. T., O. Chernomor, A. Von Haeseler, B. Q. Minh, and L. S. Vinh. 2018. UFBoot2:
 286 Improving the ultrafast bootstrap approximation. Mol. Biol. Evol. **35**: 518–522.
 287 doi:10.1093/molbev/msx281

288 Hoef-Emden, K. 2008. Molecular phylogeny of phycocyanin-containing cryptophytes:
 289 Evolution of biliproteins and geographical distribution. J. Phycol. **44**: 985–993.
 290 doi:10.1111/j.1529-8817.2008.00530.x

291 Kalyaanamoorthy, S., B. Q. Minh, T. K. F. Wong, A. Von Haeseler, and L. S. Jermin. 2017.
 292 ModelFinder: Fast model selection for accurate phylogenetic estimates. Nat. Methods
 293 **14**: 587–589. doi:10.1038/nmeth.4285

294 Koppelle, S., D. López-Escardó, C. P. D. Brussaard, J. Huisman, C. J. M. Philippart, R.
 295 Massana, and S. Wilken. 2022. Mixotrophy in the bloom-forming genus *Phaeocystis* and
 296 other haptophytes. Harmful Algae **117**: 102292. doi:10.1016/j.hal.2022.102292

297 Kumar, S., G. Stecher, M. Li, C. Knyaz, and K. Tamura. 2018. MEGA X: Molecular

298 evolutionary genetics analysis across computing platforms. *Mol. Biol. Evol.* **35**: 1547–
299 1549. doi:10.1093/molbev/msy096

300 Menden-Deuer, S., and E. J. Lessard. 2000. Carbon to volume relationships for
301 dinoflagellates, diatoms, and other protist plankton. *Limnol. Oceanogr.* **45**: 569–579.
302 doi:10.4319/lo.2000.45.3.0569

303 Minh, B. Q., H. A. Schmidt, O. Chernomor, D. Schrempf, M. D. Woodhams, A. Von Haeseler,
304 R. Lanfear, and E. Teeling. 2020. IQ-TREE 2: New models and efficient methods for
305 phylogenetic inference in the genomic era. *Mol. Biol. Evol.* **37**: 1530–1534.
306 doi:10.1093/molbev/msaa015

307 Moorthi, S. D., R. Ptáčník, R. W. Sanders, R. Fischer, M. Busch, and H. Hillebrand. 2017.
308 The functional role of planktonic mixotrophs in altering seston stoichiometry. *Aquat.*
309 *Microb. Ecol.* **79**: 235–245. doi:10.3354/ame01832

310 Nguyen, L. T., H. A. Schmidt, A. Von Haeseler, and B. Q. Minh. 2015. IQ-TREE: A fast and
311 effective stochastic algorithm for estimating maximum-likelihood phylogenies. *Mol.*
312 *Biol. Evol.* **32**: 268–274. doi:10.1093/molbev/msu300

313 Norland, S. 1993. The relationship between biomass and volume of bacteria. In: Lewis (Eds.),
314 *Handbook of Methods in Aquatic Microbial Ecology*. Lewis Publishers: Boca Raton, pp
315 303–307.

316 Parsons, T. R., Y. Maita, and C. M. Lalli. 1984. A manual of chemical and biological methods
317 for seawater analysis. Pergamon Press, Oxford.

318 Rice, E. W., R. B. Baird, A. D. Eaton, and L. S. Iles. Standard Methods for the
319 Examination of Water and Wastewater, 22nd ed., American Water Works
320 Association, Denver, CO 2012.

- 321 Solórzano, L., and H. Sharp. 1980. Determination of total dissolved phosphorus particulate
322 phosphorus in natural water. *Limnol. Oceanogr.* **25**: 754–758.
- 323 Venables, W. N. and B. D. Ripley, 2002. *Modern Applied Statistics with S*. Fourth edition.
324 Springer NY, New York.